Response of GaN to energetic ion irradiation: conditions for ion track formation

M. Karlušić,[1*] R. Kozubek,[2] H. Lebius,[3] B. Ban d'Etat, [3] R.A. Wilhelm,[4] M. Buljan,[1] Z. Siketić,[1] F. Scholz,[5] T. Meisch,[5] M. Jakšić,[1] S. Bernstorff,[6] M. Schleberger,[2] and B. Šantić[1]

[1] *Ruđer Bošković Institute, Bijenička cesta 54, 10000 Zagreb, Croatia*

[2] *Fakultät für Physik and CENIDE, Universität Duisburg-Essen, D-47048 Duisburg, Germany*

[3] *CIMAP, CEA-CNRS-ENSICAEN-UCBN, BP 5133, 14070 Caen Cedex 5, France*

[4] *Helmholtz-Zentrum Dresden-Rossendorf, Bautzner Landstraße 400, 01328 Dresden, Germany*

[5] *Universität Ulm, Institut für Optoelektronik, Albert-Einstein-Allee 45, 89081 Ulm, Germany*

[6] *Elettra-Sincrotrone Trieste, SS 14 km 163.5, 34149 Basovizza, Italy*

[*] Corresponding author: marko.karlusic@irb.hr

We investigated the response of wurzite GaN thin films to energetic ion irradiation. Both swift heavy ions (92 MeV Xe^{23+}, 23 MeV I^{6+}) and highly charged ions (100 keV Xe^{40+}) were used. After irradiation, the samples were investigated using atomic force microscopy, grazing incidence small angle X-ray scattering, Rutherford backscattering spectroscopy in channelling orientation and time of flight elastic recoil detection analysis. Only grazing incidence swift heavy ion irradiation induced changes on the surface of the GaN, when the appearance of nanoholes is accompanied by a notable loss of nitrogen. The results are discussed in the framework of the thermal spike model.

Keywords: GaN, swift heavy ion, highly charged ion, ion track, thermal spike

1. INTRODUCTION

Over the past two decades, GaN has proven to be a useful and reliable material for various electronic and optoelectronic applications, particularly for blue and violet light emission. White light emitting diodes based on GaN are well established on the market and have become a part of everyday life. This created considerable interest for the investigation of various phenomena related to GaN.

Interactions of energetic ions with GaN are interesting both for processing and for the study of sustainability of devices based on GaN. The response of GaN to ion irradiation has been investigated previously but mostly for low energy ions, when the nuclear energy loss is the dominant energy transfer mechanism [1,2]. Despite the importance of this material and its known reliability in harsh radiation environments [3,4], only a few reports are available in which the response of GaN to high energy ions, i.e. swift heavy ions (SHI) was studied [5-10]. The reason for the present situation is that in comparison to insulators, semiconductors are less prone to this kind of radiation damage [11-13] and have thus not been extensively studied.

The response of GaN to another class of energetic ions, namely highly charged ions (HCI), has also been investigated before. A significant erosion of the surface was observed for a potential energy (defined as the sum of the ionizing energies) above 7 keV [14]. However, large fluencies in the range of $10^{14} – 10^{16}$ ions/cm^2 used in the work of Zhang *et al.* yield a pre-damaged surface area (due to unavoidable elastic ion collisions with surface atoms) which could strongly influence erosion driven by the potential energy of the HCI. Therefore, low fluence experiments are essential to elucidate the response of non-damaged GaN surfaces to individual HCI impacts.

In the present work, we report the results of our investigations regarding SHI and HCI irradiation of GaN. The irradiation effects were investigated using atomic force microscopy (AFM), grazing incidence small angle X-ray scattering (GISAXS), Rutherford backscattering spectroscopy in channelling orientation (RBS/c) and time of flight elastic recoil detection analysis (TOF-ERDA). The irradiation parameters were chosen to investigate the response of GaN close to the so called “ion track formation threshold”, and to complement previous work performed with higher energy SHI beams [5-8]. In addition, grazing incidence SHI irradiation [15-17] was applied in order to study the response of the GaN surface in particular. Possible compositional changes in this case were investigated by TOF-ERDA which is sensitive to a possible nitrogen loss which has been reported previously for this material [18-20]. Our results are interpreted in terms of the material changes predicted by the thermal spike model [21,22].

2. MATERIAL RESPONSE TO ENERGETIC IONS

The passage of a swift heavy ion (SHI) through a solid material can result in permanent damage along the ion’s trajectory and is commonly called an ion track [12,13,23-25]. The most common description of the ion track formation, the thermal spike model, suggests that the considerable kinetic energy of the projectile (in the MeV – GeV range) is predominantly deposited in the form of a dense electronic excitation along the trajectory and can thus lead to localised melting of the material. The density of the deposited energy is given by the electronic energy loss (S_e) of the SHI that can be evaluated by the SRIM code [26]. In contrast, the nuclear energy loss is small and can be neglected in this energy regime. Upon rapid quenching due to the large temperature gradient between the molten track and the surrounding cold matter, the melt may resolidify in an amorphous phase along the ion

trajectory. Increasing the intensity of the electronic excitation by using heavier and more energetic ion beams results in a spatially extended molten zone. Consequently, wider ion tracks are observed. On the other hand, if the electronic excitation is not sufficiently intense, melting may not occur, and the deposited energy dissipates away leaving the material almost unaltered. Therefore, the energy threshold for ion track formation (S_{et}) and the track size both depend on the ion beam parameters and material properties.

Despite their nanometric sizes, ion tracks in the bulk can be observed with several techniques. The techniques most often used are transmission electron microscopy (TEM) and Rutherford backscattering spectroscopy in the channelling mode (RBS/c) [5,17,27,28]. TEM offers the possibility for direct observation of the ion tracks, but the procedure is not simple and not many samples can be examined readily. RBS/c measures the ion track size indirectly by observing the fraction of amorphised material in the crystal matrix, as a function of the applied SHI fluence. With some exceptions, the agreement between these two techniques is good [27]. Only for very small ion tracks with radii less than 2 nm, RBS/c yields lower values of the ion track sizes than TEM because such small tracks tend to be discontinuous. Analyzing ion tracks in amorphous materials is even more challenging, but recently other techniques like small angle X-ray scattering (SAXS) and infrared spectroscopy (IR) were found to be applicable [29-35].

In radiation sensitive material, at the position of the ion impact, typically surface ion tracks in form of nanohillocks or craters can be observed by using scanning probe microscopy techniques like atomic force microscopy (AFM) [23]. Similar to ion tracks in the bulk, there is always a threshold for nanohillock formation. Above this threshold, nanohillocks grow in size with increasing ion energy. Similar values for the threshold for ion tracks in the bulk and on the surface have often been observed [17,36,37], thus enabling to analyse the threshold with two complementary techniques. SHI irradiation under grazing incidence angles increases the near-surface interaction volume and therefore induces even more dramatic changes on the material surface. In this case individual single ions may produce long chains of evenly spaced nanohillocks [15-17,38].

Slow highly charged ions (HCI) as another class of energetic ions can also induce changes on the sample surface because their potential energy due to the large number of missing electrons is often sufficient to induce surface nanostructures in many materials via electronic excitations [23]. Given the similarities between SHI tracks and HCI induced surface nanostructures (material modification due to dense electronic excitation, threshold for track formation E_{pt}), the thermal spike concept was also extended to this field [22,39,40]. For brevity and simplicity, here we refer to HCI induced surface nanostructures as 'HCI tracks' even though the ion's potential energy is deposited in a point-like volume rather than in an elongated track - in contrast to SHI.

3. EXPERIMENTAL DETAILS

Wurzite GaN thin film samples were grown by low-pressure metalorganic vapor phase epitaxy on *c*-plane sapphire substrates at the University of Ulm following an optimized procedure for low defect density material [41]. The layer thickness was 3 μm with a surface RMS roughness of <0.15 nm. SHI irradiations were performed at the IRRSUD beamline at GANIL, Caen (France) using 92 MeV Xe^{23+} ions. A second set of SHI irradiations was done at the RBI, Zagreb (Croatia) using 23 MeV I^{6+} ions. The ion beams were scanned using magnetic coils to achieve homogenous irradiation of the samples. All irradiations were done at room temperature. Normal and grazing incidence irradiation geometries were used. To avoid channelling of the SHI, normal incidence irradiation was done at 6° with respect to the *c*-axis, while grazing incidence irradiation was done at 1° with respect to the surface, in the m-crystallographic direction ([10-10]). The applied fluencies were up to 10^{13} ions/cm^2 (IRRSUD), up to 10^{14} ions/cm^2 (RBI) for normal incidence irradiation, and up to 10^{10} ions/cm^2 for grazing incidence irradiation. Additionally, HCI irradiation was done at UDE, Duisburg (Germany), with Xe^{40+} under normal incidence with a fluence of 10^{10} ions/cm^2 and kinetic energy of 100 keV [42]. Relevant ion beam parameters are given in Table 1. For HCI it is not possible to calculate the electronic energy loss using the SRIM code [26], but a recent study indicates that the energy loss of such a projectile can be up to 10% of its kinetic energy when passing through 1 nm thin membrane [43].

TABLE 1. Irradiation parameters used in this work. Energy losses were calculated using the SRIM 2013 code [26].

Ion	Kinetic energy (MeV)	Potential energy (keV)	Electronic energy loss (keV/nm)	Nuclear energy loss (keV/nm)	Angle	Fluence (ions/μm^2)	Irradiation facility
Xe^{23+}	92	6.5	22.8	0.2	84º	$10^3 – 10^5$	IRRSUD
Xe^{23+}	92	6.5	22.8	0.2	90º	100	IRRSUD
Xe^{23+}	92	6.5	22.8	0.2	1º	5, 100	IRRSUD
Xe^{40+}	0.1	38.5	N/A	4	90º	100	UDE
I^{6+}	23	0.2	7.8	0.6	84º	$10^4 – 10^6$	RBI
I^{6+}	23	0.2	7.8	0.6	1º	5, 100	RBI

Surface modifications were inspected by tapping mode AFM performed under ambient conditions using a Dimension 3100 AFM (Veeco Metrology, Santa Barbara, CA, USA) and NCHR cantilevers (Nanosensors, Neuchatel, Switzerland) with cantilever resonance frequencies around 300 kHz. Images were analysed using the WSXM code [44]. From the raw data (512x512) only a parabolic background was subtracted.

The analysis of surface ion tracks was complemented by a novel approach using GISAXS. This experiment was carried out at the synchrotron facilities of Elettra-Sincrotrone Trieste, Italy on the SAXS beamline [45], using

synchrotron radiation with wavelength λ=0.154 nm (photon energy of 8 keV). The grazing angle of incidence was selected to be slightly above the critical angle for total reflection. A two dimensional image plate detector with 2000x2000 pixels, positioned perpendicular to the incident beam at a detector to sample distance L=1800 mm, was used to record the SAXS intensity. A thin, partly transparent Al strip was placed in front of the 2D detector in order to avoid saturation in the specular plane direction where the usually much stronger surface scattering is present.

Swift heavy ion tracks in bulk GaN, formed after normal incidence irradiation, were investigated with RBS/c using 1.7 MeV He ions delivered by a 2 MV Van de Graaff accelerator located at the Ion Beam Center of the Helmholtz-Zentrum Dresden-Rossendorf. A beam spot size of 1 mm^2 was chosen by means of a collimator and the ion beam current was kept below 10 nA. The backscattered particles were detected in a silicon surface barrier detector with 15 keV energy resolution located at 170° with respect to the incoming beam. The alignment of each analyzed sample was achieved by obtaining characteristic RBS/c spectra from an unirradiated part of the sample. The samples were not coated with a conducting layer, although this is a common procedure to avoid a charge build-up during analysis [28]. However, the low current of the analysing beam and the quality of the RBS/c spectra of the virgin samples was sufficient to justify the omission of this step.

To investigate possible stoichiometric changes of the GaN, *in situ* TOF-ERDA measurements were performed at the RBI using a 23 MeV I^{6+} beam at 20° and 1° grazing angle of incidence with respect to the sample surface. The TOF-ERDA spectrometer [46-48] was positioned at an angle of 37.5° toward the beam direction. All data were collected in the "list mode" and offline replay/analysis with sections was performed using the Potku software package [49]. The total number of ions hitting the sample was calculated using the known solid angle of the detector and the charge × solid angle product determined by simulating the energy spectra of Ga and N using the simulation code SIMNRA [50].

4. RESULTS

4.1. Atomic force microscopy (AFM)

Grazing incidence SHI irradiation induces pronounced changes on the GaN surface where chainlike surface ion tracks were observed. In contrast to our previous work on other materials [15-17,38], where only nanohillocks were found, the morphology of the 92 MeV Xe^{23+} surface ion tracks on the GaN surface contains both nanohillocks and as a new feature nanoholes (Fig. 1a, b). Since the beam direction of the SHI was always from the top of the AFM images, we conclude that at these values of energy loss, surface ion tracks typically start with a series of nanoholes, and only later, when the SHI penetrates deeper into the material, nanohillocks can appear. For heavier and more energetic ions (104 MeV Pb^{28+}, S_e = 24 keV/nm, grazing angle = 1°) only nanohillocks have been

observed earlier [8]. On the other hand, after 23 MeV I^{6+} (S_e = 7.8 keV/nm) irradiation, we observed that the surface ion tracks consist only of nanoholes (Fig. 1c). This same morphology of surface ion tracks was also observed in contact mode AFM (not shown here) and similar features were probably also observed earlier (74 MeV Kr^{18+}, S_e = 17 keV/nm) [8]. Therefore, we conclude that two thresholds for surface ion tracks exist: one below 8 keV/nm when only nanoholes are produced, and the other, around 20 keV/nm, when nanohillocks appear as well. This is probably the reason why surface ion tracks consisting of only nanoholes are also sometimes observed after 92 MeV Xe^{23+} irradiation, because the electronic energy loss of 92 MeV Xe^{23+} is very close to the second threshold and both kinds of SHI track morphologies are likely to appear.

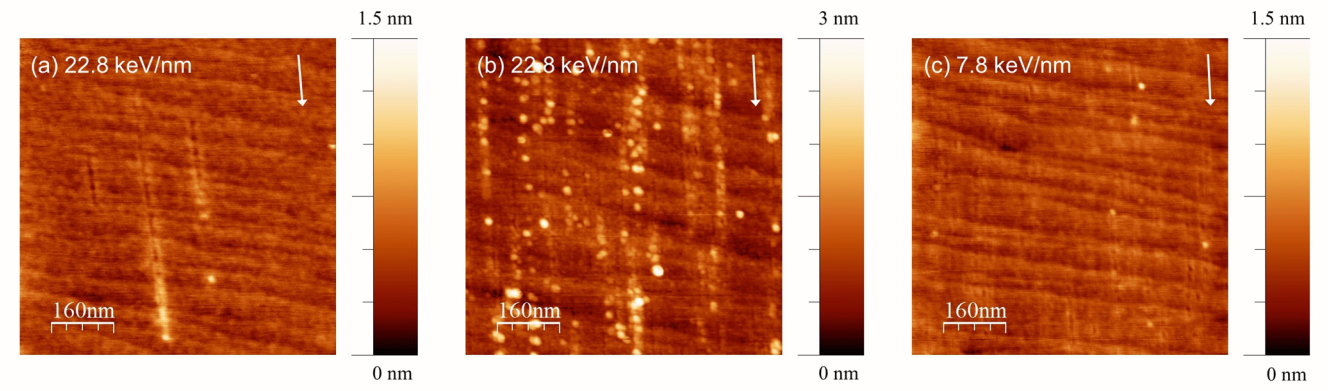

Figure 1. AFM images of the GaN surface after 1° grazing incidence irradiation using (a) 92 MeV Xe^{23+}, fluence 5×10^8 ions/cm^2 (b) 92 MeV Xe^{23+}, fluence 1×10^{10} ions/cm^2 and (c) 23 MeV I^{6+}, fluence 1×10^{10} ions/cm^2. The white arrow marks ion beam direction.

In contrast, after normal incidence irradiation with 92 MeV Xe^{23+} ions, very few nanohillocks were observed on the GaN surface, see Fig. 2a for a typical AFM image. The efficiency for the nanohillock production is estimated to be below 1%, since the applied fluence was 10^{10} ions/cm^2, and typically only few nanohillocks were observed. Such an extremely low efficiency indicates that the irradiation conditions are below the threshold for nanohillock formation. In the case of HCI irradiation, at this resolution no surface tracks were observed after Xe^{40+} irradiation with a fluence of 10^{10} ions/cm^2 and kinetic energy of 100 keV (Fig. 2b).

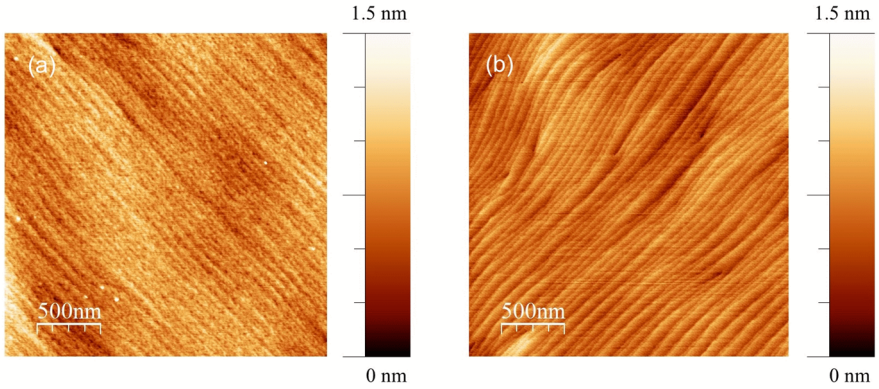

Figure 2. AFM images of the GaN surface after normal incidence irradiation using (a) 92 MeV Xe^{23+} and (b) 100 keV Xe^{40+}. The diagonal lines are terraces and surface steps, respectively. Despite a fluence of 10^{10} ions/cm^2 only very few (a) or even no features at all (b) are detected.

4.2. Grazing incidence small angle X-ray scattering (GISAXS)

The structural properties of the GaN surfaces irradiated by SHIs at grazing angle were analysed by the GISAXS technique [32,33]. GISAXS intensity distributions measured on differently treated surfaces are shown in Fig.3. All maps show significant intensity originating from the surface ion tracks shown in Fig. 1. GISAXS maps measured for three different angles between the probing X-ray beam and ion-track directions (denoted by ϕ) are shown for each sample. The maps of the GaN surface irradiated with 92 MeV Xe^{23+} ions, fluence 5×10^8 ions/cm^2 are shown in Figs. 3. (a)-(c). When the X-ray beam is parallel to the ion tracks (ϕ =0º), the maps are symmetric, while a characteristic tail is present for the non-parallel orientations. The analysis of the GISAXS maps has been performed using two modified paracrystal models developed for the analysis of ion tracks formed on irradiated surfaces [51].

The simulations using the first model are shown in the insets of Figs. 3(a)-(c). The model assumes that ion tracks are randomly distributed on the surface. Each track consists of nanostructures formed along the trajectory during the ion passage. The arrangement of nanostructures within each track is described by a basis vector $\boldsymbol{a}_1$ directed along the track (x direction). The number of the periods (i.e. the number of nanostructures along the track) of $\boldsymbol{a}_1$ is denoted by N_x, so the average ion track length is $N_x\,|\boldsymbol{a}_1|$. Such a geometry is assumed in accordance with the AFM measurements showing the formation of ordered nanostructures along the ion tracks. The deviations from the ideal positions defined by $\boldsymbol{a}_1$ are described by two parameters: σ_1 which describes the deviation in the direction along the track (the nanostructures are assumed to have a short range order in this direction) and σ_2 which describes the deviations of the nanostructure positions perpendicular (y direction) to the ion tracks. The nanostructures are assumed to deviate from the ideal positions (centre of ion track) according to a normal distribution with a standard deviation of $\sigma_{1,2}$ /2 [51]. The nanostructures are assumed to have an elliptical shape

described by the radii R_x, R_y and R_z. The best fit for all three maps was obtained using the following parameters: $|\boldsymbol{a}_1|$= 50 ±10 nm, N_x=12±4, R_x=4±1 nm, R_y=1.9±0.3 and R_z=1.2 ±0.3 nm. The standard deviation of the size distribution was found to be 0.6±0.2 nm, while the disorder parameters are σ_1= 34±2 nm and σ_2= 0.4±0.2 nm.

The GISAXS maps of the GaN surface irradiated with 92 MeV Xe^{23+}, fluence 1×10^{10} ions/cm^2 are shown in Figs. 3(d)-(f). It is interesting to note two lateral peaks located at nearly $|Q_y|$=0.5 nm^{-1} that are present in the GISAXS maps and indicated in Fig. 3(d) by arrows. These peaks show that the separation between the ion tracks exhibits short range ordering, probably related to the higher fluence applied. Therefore we use a second model to describe this observed GISAXS intensity distribution. In addition to the assumptions presented above (our first model), we assume now that the tracks are separated by a basis vector $\boldsymbol{a}_2$ oriented perpendicular to the ion tracks instead of the random separation which was used for the first model. The distribution of the deviations of the positions of the ion track from the ideal ones (defined by $\boldsymbol{a}_2$) in y direction are described by the third disorder parameter σ_3. The analysis of the maps shows that the characteristic separation between the tracks ($|\boldsymbol{a}_2|$) is 9.1 ±0.8 nm and σ_3= 5.3 ±0.8 nm. The other parameters are very similar to the ones obtained for lower irradiation fluence.

The results of the GISAXS analysis agree well with the available AFM data for 92 MeV Xe^{23+} irradiation (ion track length 200-500 nm, inter-hillock distance 40-50 nm, height of the nanohillocks ~ 1 nm). However, the analysis of the AFM images is not straightforward because the periodicity of the ion tracks is much less pronounced than for example in $SrTiO_3$ [17]. Hence GISAXS is a valuable tool that can provide ion track parameters with more reliability. Also, effects related to the AFM tip size are avoided, which could be important in particular for the nanohole characterisation.

Finally, we analyse the GISAXS maps of the GaN surface irradiated with 23 MeV I^{6+}, fluence 1×10^{10} ions/cm^2 (Fig. 3(g)-(i)). Although the tracks are hardly visible by AFM (Fig. 1c), their presence is clearly evident in the corresponding GISAXS maps. The characteristic tails are well visible; however, their relative intensity is significantly lower than for the 92 MeV Xe^{23+} ion irradiation. The map of the non-irradiated sample (shown in the inset of Fig. 3 (i)) shows no tails, only very low diffuse scattering excluding the intensity close to Q_y=0 which originates mostly from the surface roughness contribution. The analysis of the GISAXS maps shows the presence of nanostructures with characteristic separation of 8±1 nm, similar to the case of irradiation with higher fluence of 92 MeV Xe^{23+} ions. The standard deviation of the characteristic separation is σ_3= 4±1 nm for this case. According to the GISAXS analysis, R_x is found to be larger than 4 nm, indicating that the formed nanostructures can be even connected along the ion tracks. However, the data obtained by GISAXS in this case are not very accurate due to the low signal originating from the tracks with respect to the signal coming from the surface roughness of the unaffected area.

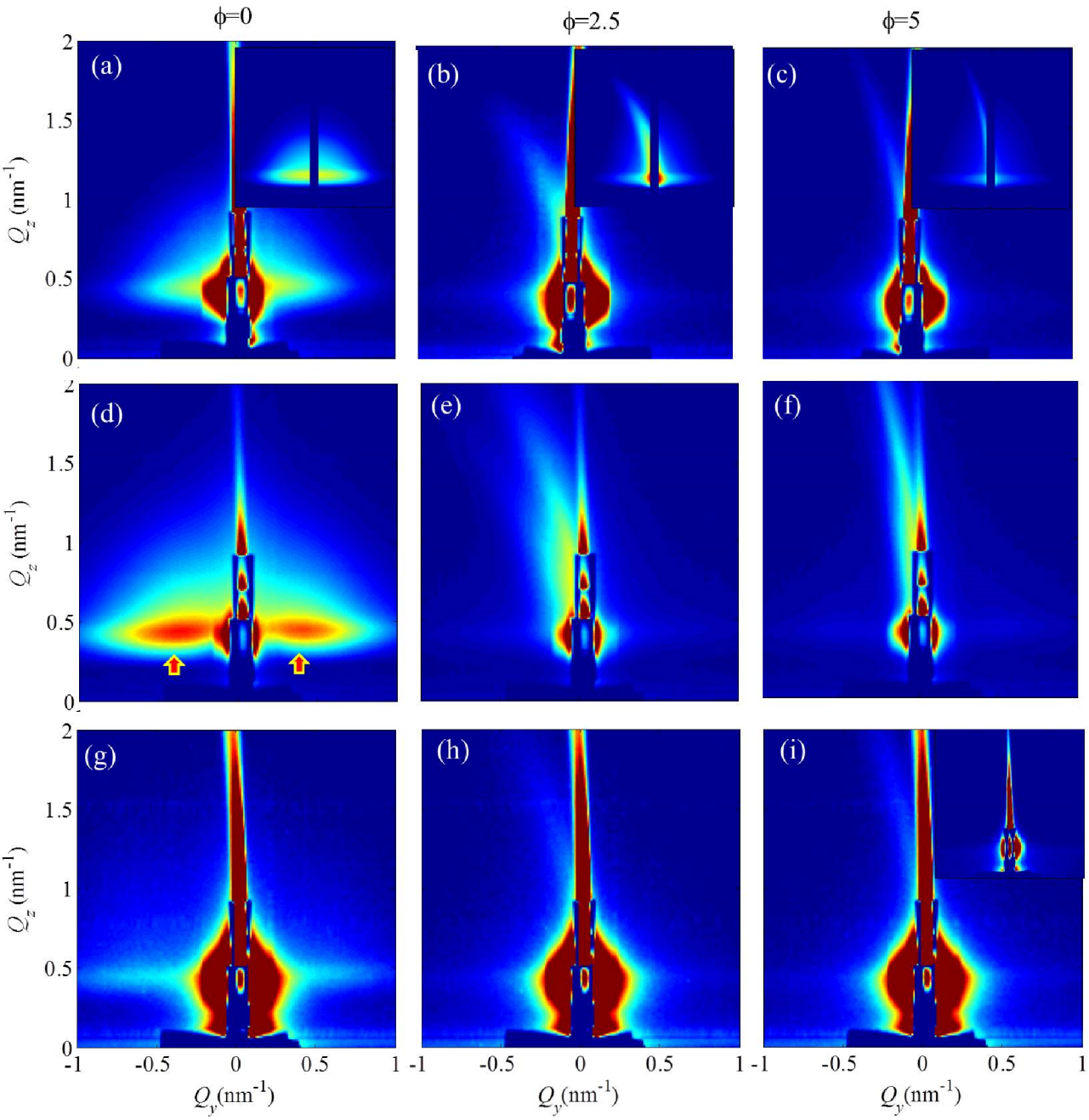

Figure 3. GISAXS maps of: (a)-(c) 92 MeV Xe^{23+}, fluence 5×10^{8} ions/cm^2, the insets show simulations of the measured GISAXS maps. (d)-(f) 92 MeV Xe^{23+}, fluence 1×10^{10} ions/cm^2, (g)-(i) 23 MeV I^{6+}, fluence 1×10^{10} ions/cm^2. The inset in Fig. (i) shows a GISAXS map of the non-irradiated sample for comparison.

4.3. Rutherford backscattering in channelling (RBS/c)

The presence of ion tracks can be detected using RBS/c since the amorphised fraction of the initially crystalline sample enhances the yield of backscattered He ions. To calculate the ion track radii, a surface approximation is often used, where a linear fit of the high energy part of the RBS/c spectra allows to determine the backscattering yield at the position of the surface peak [27,52]. By comparing this backscattering yield to the same yield when RBS/c is done in a random orientation, the fraction of the amorphised material can be calculated. The radii of the ion tracks (assuming they have identical sizes and cylindrical symmetry) can then be derived from Poisson's law that describes the evolution of the amorphisation with the applied SHI fluence.

The results presented here show that no tracks were observed in GaN after normal incidence 23 MeV I^{6+} and 92 MeV Xe^{23+} ion irradiation, even after the exposure to the highest fluences of $10^{14}/cm^2$ and $10^{13}/cm^2$, respectively (Fig. 4). All of the recorded RBS/c spectra are almost identical to the spectra obtained on the virgin (i.e. not irradiated) sample, therefore we conclude that the Ga sublattice remains intact. Slight dechanneling observed in the RBS/c spectrum of the sample irradiated using 92 MeV Xe^{23+} with the highest fluence ($10^{13}/cm^2$) indicates a small amount of subthreshold damage because the backscattering yield at the position of the surface peak vanishes.

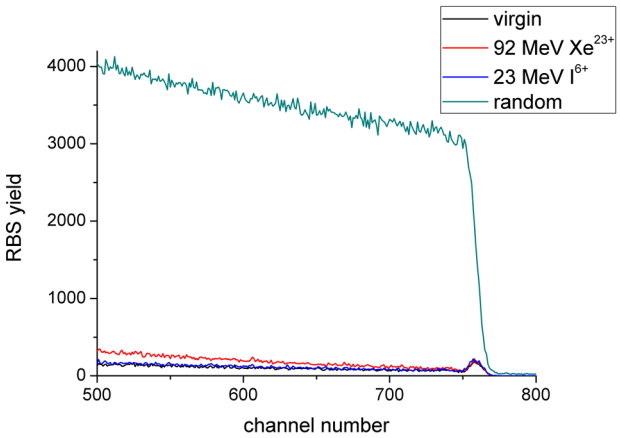

Figure 4. RBS/c spectra from the samples irradiated by 92 MeV Xe^{23+} with fluence $10^{13}/cm^2$ (red) and 23 MeV I^{6+} with fluence $10^{14}/cm^2$ (blue). For comparison, RBS/c spectra from the unirradiated sample in channeling (black) and in random geometry (magenta) are also shown.

4.4. Time of Flight - Elastic Recoil Detection Analysis (TOF-ERDA)

In a TOF-ERDA analysis, the atomic composition and the depth profiles of all elements present in the sample can be measured in just one run. The energy spectra of each element are converted to a depth profile using known electronic energy loss data and scattering cross sections. Since the experimental data are collected in the "list mode" (event by event), compositional changes of the sample due to elemental losses (caused by primary beam irradiation) can be easily monitored. In contrast to ref. [18], where nitrogen depletion of GaN samples was observed during ERDA using 200 MeV Ag (S_e = 26 keV/nm) ions at 20° angle between incoming ion and sample surface, an offline replay shows that the nitrogen content within the first 5 nm seems to be stable during 23 MeV I^{6+} irradiation up to a fluence of 5×10^{12}/cm^2 at the same angle of 20º. However, the offline analysis of the TOF-ERDA measurement performed using 23 MeV I^{6+} at a grazing incidence angle of 1° shows a significant loss of nitrogen from the first 8.5 nm already at the fluence of 2×10^{11}/cm^2 (Fig. 5).

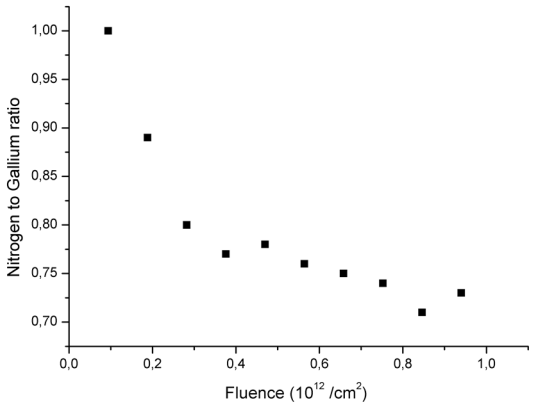

Figure 5. Nitrogen-to Gallium ratio calculated from an offline analysis of in-situ TOF-ERDA measurements performed by 23 MeV I^{6+} ions at 1° grazing incidence angle. A significant loss of nitrogen is evident.

5. DISCUSSION

5.1. Grazing incidence irradiation

Irradiation of crystalline materials using SHI at grazing incidence angles is known to result in elongated surface ion tracks, sometimes with prominent, equally spaced nanohillocks along the SHI trajectory [15-17,38]. An explanation for their occurrence was given within the thermal spike model by taking into account that the electronic energy loss of SHI oscillates when it traverses a crystal at grazing incidence angle. The oscillating electronic energy loss of the SHI is due to encounters with regions of different electron densities along its trajectory when passing through the crystal planes [53]. The transfer of the SHI energy loss into the material via electron phonon coupling results in localized melting along the SHI trajectory [15]. Upon rapid quenching, distinct

nanohillocks are formed, as demonstrated for several insulating materials like CaF_2, SiO_2, etc. [38]. Thus, our findings as shown in Fig. 1 are in principle in line with these earlier studies.

While the hillocks are generally interpreted as a signature of molten material, the occurrence of holes (see Fig.1) clearly indicates a loss of material. Very recently, it was shown that in case of another wide band gap material, silicon carbide (SiC), grooves with a depth of ~ 0.3 nm instead of chains of nanohillocks appear [54] when irradiated by SHI under grazing incidence angle. In a broader context, the observation of nitrogen loss reported here and the loss of silicon from the SiC surface upon SHI irradiation reported in ref. [54] opens up the question of the composition of SHI tracks. The underlying material modification mechanism is different compared to classical experiments of sputtering the material by SHI in the electronic energy loss regime, when secondary ions are detected after large incidence angle irradiation, and when sputtering is assigned to vaporisation of the material [55]. In case of SiC, spatially resolved thermal spike calculations [54] indicate that surface ion tracks are formed where the temperature increase is above the required temperature for SiC decomposition. It is known that GaN undergoes decomposition via nitrogen loss when heated above 900 °C [56,57], so it is indeed very likely that a similar mechanism takes place at low stopping powers (23 MeV I^{6+}). At higher stopping powers however (92 MeV Xe^{23+}) the formation of hillocks, i.e. fully developed surface SHI tracks (Fig. 1b) occur in GaN, because now the thermal spike overcomes the melting temperature of around 2500 °C. Because SiC is a very radiation hard material [58,59], the latter mechanism is inactive, and thus only decomposition by sublimation takes place.

To describe the SHI track formation on the surface produced after grazing incidence irradiation, several important issues have to be considered. A major channel of energy dissipation at the surface is the loss of primary electrons that carry energy away from the material; hence not all kinetic energy of the SHI is deposited into the material. This effect should be most pronounced close to the track formation threshold. Ejected electrons could also promote a Coulomb explosion mechanism because charge imbalance close to the place of the SHI impact would prolong the time during which this mechanism is active. Mass removal, as observed in case of SiC [54] and GaN (Fig. 5), can also be an important channel for energy dissipation. In addition, the surface acts as a heat flux reflector, hence the achieved temperatures can be higher due to the confinement effect [60].

Both our GISAXS and AFM measurements have shown that grazing angle SHI irradiation yields pronounced surface tracks. These measurements reveal that the surface tracks in GaN, be it hillocks or holes, exhibit a periodic pattern. In crystalline materials the oscillating energy loss of the SHI during penetration into the material under grazing incidence can have peak values much higher than the average values calculated by the SRIM code [53]. The wurzite structure of GaN could promote this effect even more, as shown in Fig. 6. The crystal planes normal to the *c*-axis are grouped into Ga-N bilayers, which are separated by a distance three times larger than the bilayer's thickness. In addition, 3/4 of the bonding electrons are contained in the bilayers. When a grazing ion penetrates through such a bilayer, it encounters densely packed atoms and bonding electrons (Fig. 6a). Since the grazing angle is typically 1º (see the cyan line in Fig. 6), the energy deposition is high along the track within a bilayer. On the other hand, for normal incidence, an ion encounters hexagonal openings along the *c*-axis. Due to the slightly larger angle (6º off the normal axis) chosen in our experiment, an ion encounters only a few atoms before its

trajectory switches to the other side of the hexagonal tube or to the neighbouring hex-tube. A side view of such an ion trajectory is shown in Fig. 6(b). Therefore, due to the choices of the angles, 1° with respect to the *c*-plane for grazing incidence and 6° with respect to the *c*-axis for normal incidence, and due to the GaN quasi-layered structure, the energy depositions along those exemplary trajectories are quite different. For normal incidence smaller energy packages are released at higher frequency, making the energy deposition more uniform and stretched along the trajectory. For grazing incidence, larger energy packages are released each time the ion transits through a bilayer. We assume this to be the main reason why ion tracks on the surface accompanied by the nitrogen loss are observed after grazing incidence irradiation even at lower SHI energies (23 MeV I^{6+}, see Figs. 1c, 3g-i and 5).

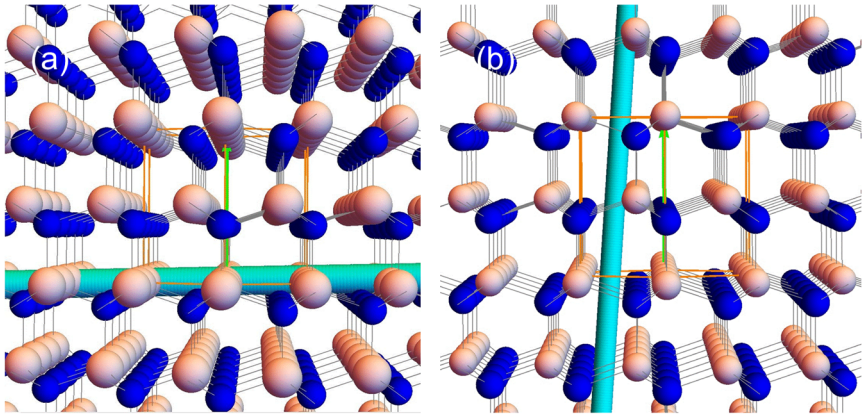

Figure 6. (a) Wurzite GaN crystal lattice, reddish and blue balls represent Ga and N atoms, respectively. Orange lines designate the standard unit cell. The *c*-axis (green arrow) points upwards. The cyan line illustrates the grazing trajectory, inclined by 1° with respect to the *c*-plane. (b) Side view of an ion trajectory inclined by 6° with respect to the *c*-axis (green arrow).

From a more general point of view, the present study demonstrates the possibilities for ion track based applications like surface nano-patterning [15,17] and the production of rippled substrates [61] at smaller ion accelerator facilities. The relevant parameter for material modification using SHI is the electronic energy loss which is not linear with respect to the kinetic energy of the ion. By performing irradiations at grazing incidence angle, when the peak values of the oscillating energy loss exceed the average energy loss values to a large extent, the use of smaller ion accelerator facilities could be extended to an even wider range of materials. The availability of advanced ion beam analysis techniques like TOF-ERDA is an additional valuable asset for *in-situ* analysis.

5.2. Normal incidence irradiation

Our RBS/c and AFM measurements showed that normal incidence irradiation using SHIs does not result in the formation of ion tracks, neither on the GaN surface nor in the bulk. Similarly, after normal incidence irradiation using HCIs, surface HCI tracks were also not observed. These results thus provide a lower limit for SHI track formation threshold of $S_{et} > 22.8$ keV/nm, and for HCI track formation threshold of $E_{pt} > 38.5$ keV. In the following we will discuss the relevance of these findings in the frame of the thermal spike model.

The analytical thermal spike model (ATSM) [62] provides a simple estimate for the SHI track formation threshold (Eq. 1) and a recent extension of the same model [22] provides an estimate for the HCI track formation threshold (Eq. 2):

$$S_{et} = \frac{\rho c \pi a^2(0) \Delta T_m}{g} \quad (1)$$

$$E_{pt} = \frac{\rho c \left(\sqrt{\pi} a(0)\right)^3 \Delta T_m}{2g} \quad (2)$$

According to the model, thresholds can be calculated in terms of electronic energy loss of the SHI or potential energy of the HCI using thermodynamic parameters of the given material (density ρ, specific heat capacity c given by the Dulong-Petit law and the temperature increase to achieve melting ΔT_m) and the model parameters $a(0)$ and g. The model parameters $a(0)$ and g can be interpreted as the initial width of the thermal spike having a Gaussian profile and the fraction of the energy deposited into the material due to the SHI impact that transfers into the thermal spike, respectively. Standard model parameters for the SHI tracks in insulators are $a(0) = 4.5$ nm and $g = 0.4$ for low velocity irradiation ($E_{kin} < 2$ MeV/nucleon). In case of SHI tracks in semiconductors, these values should be different: $a(0) = 9$ nm is expected for GaN because its bandgap is $E_g = 3.4$ eV and $g = 0.2$ is expected even for low velocity irradiations [21]. For the HCI tracks, the threshold potential energy can be calculated using Eq. (2) but the values of the model parameters $a(0)$ and g are still an open question in the case of semiconductors [22].

TABLE 2. Experimental data on SHI ion tracks in GaN. Energy losses were calculated using the SRIM 2013 code [26].

Ion	Kinetic energy (MeV)	Electronic energy loss (keV/nm)	Ion track radius (nm)	Characterization technique	Reference
Xe^{23+}	92	22.8	0	RBS/c	Present work
Pb^{32+}	132	28.3	1.5	HREM	[7]
Au^{16+}	200	34.3	4.5	RBS/c	[5]
Au^{16+}	200	34.3	5	TEM	[5]
Pb^{27+}	230	36.5	2.4	RBS/c	[6]

We begin by discussing the SHI case, where experimentally determined track radii may be used to extract $a(0)$ and g, using the available literature data on SHI tracks in GaN (compiled in Table 2) and known material parameters of GaN (ρ = 6.15 g/cm^3, c = 0.6 J/gK, ΔT_m = 2500 °C). We have not observed ion tracks after 92 MeV Xe^{23+} irradiation, and very small ion tracks were observed after 132 MeV Pb^{27+} irradiation [7]. Therefore, the threshold for SHI track formation is between 22.8 keV/nm and 28.3 keV/nm, which is rather high. The analysis of the data from Table 2, using a procedure as outlined in ref. [62], yields the model parameters $a(0) = 8.5 \pm 1.9$ nm and $g = 0.51 \pm 0.08$. As expected for semiconductors, the parameter $a(0)$ is larger than the standard value for insulators ($a(0)$ = 4.5 nm), with a value close to the one predicted in ref. [21]. The value of g is more in line with the expectations for the insulator response to SHI irradiation (g = 0.4). Still, more experimental data is needed to evaluate both model parameters with better accuracy. For example, high velocity experiments (E_{kin} > 8 MeV/nucleon) could clarify this issue, because in this case g should have a low value regardless of the material under investigation [21]. Different g values found at high and low velocity experiments would then provide evidence for a possible contribution from Coulomb explosion at low velocities, which is a typical response of insulators.

Next, we address the HCI case, where both model parameters may be different from the standard values. To obtain upper boundaries for the model parameters, HCI irradiations with sufficiently high charge states that induce observable surface ion tracks would be needed. However, GaN has a very high threshold for HCI track formation compared to other inorganic crystalline materials, see the compilation in Fig. 7. In this compilation we omitted results from HCI irradiations of layered materials like mica, HOPG and recently MoS_2 [63] because of their anisotropic transport properties that can influence the thermal spike [64] and may result in a shift of the track formation threshold. From Fig. 7 one can see that recently obtained experimental data points for $LiNbO_3$ [65], BaF_2 [66] and Al_2O_3 [67], together with the present new data for GaN, exhibit a large scatter. This is different from an earlier study where a more uniform threshold behavior for a variety of other materials was found [22]. The reason for this may be the different and in part high kinetic energy of the HCI used in the various studies. The velocity of the projectile will certainly influence the energy deposition and thus the track formation [68-70]. For this reason a systematic study with HCI at very low kinetic energies [39] would be helpful. Still, in contrast to SHI tracks [71-74], it seems that the investigated materials do not show the same uniform response with respect to HCI track formation. As can be seen from Fig.7, especially more experimental work on HCI irradiation of TiO_2 (rutile) and Al_2O_3 would be of interest. Track formation below E_{pt} = 11 keV for TiO_2 and below E_{pt} = 16 keV for Al_2O_3 is forbidden according to Eq. (2) because of energy conservation ($g \leq 1$), so this could be a chance to test the ATSM.

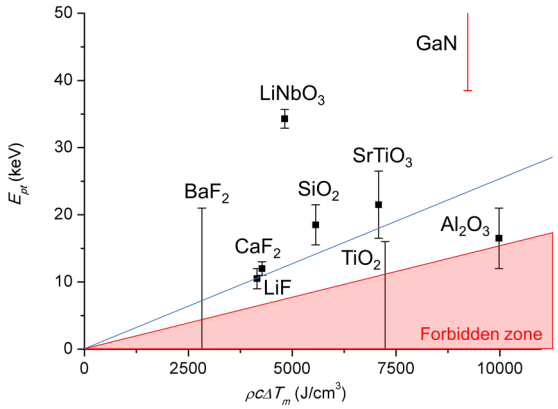

Figure 7. Experimentally determined thresholds for HCI track formation (nanohillocks) in different inorganic crystalline materials from ref. [22] updated with data for $LiNbO_3$ [65], BaF_2 [66], Al_2O_3 [67] and GaN (present work, in red). According to the ATSM, the formation of HCI tracks should be forbidden in the area marked in red. The blue line presents the expected HCI track formation threshold in insulators ($a(0)$ = 4.5 nm, g = 0.64).

Finally we compare the threshold values found for SHI and HCI irradiations. The ion tracks in both cases stem from dense electronic excitations and usually show similar surface features [22,23]. These obvious similarities have led to the idea that the physical mechanisms are essentially the same and at least for insulators, there should be a relationship between the track formation thresholds for SHI and HCI based on eqs. (1) and (2). More precisely, assuming $a(0)$ = 4.5 nm for both SHI and HCI tracks, and g^{SHI}/g^{HCI} = 0.625 [22], their ratios should be given by the following estimate:

$$\frac{E_{pt}}{S_{et}} = \frac{a(0)\sqrt{\pi}}{2}\frac{g^{SHI}}{g^{HCI}} = 2.5\ nm \qquad (3)$$

A large majority of insulating materials indeed shows an E_{pt}/S_{et} ratio around 2.5 nm [22] as predicted by eq. (3). In particular, other wide bandgap semiconductors with similar energy bandgap values as GaN (E_g = 3 eV for both $SrTiO_3$ and TiO_2) follow eq. (3). Therefore, with the threshold for SHI track formation S_{et} determined to be around 25 keV/nm in GaN, a threshold for HCI track formation above E_{pt} = 38.5 keV is not surprising. However, the much higher SHI track formation threshold in GaN as compared to $SrTiO_3$ and TiO_2, as well as only approximately known values of the ATSM model parameters *a(0)* and g for GaN, makes any more specific predictions too speculative at this point. For this, clearly more experimental work on the response of GaN to energetic ions is needed.

VI. CONCLUSION

We have investigated the response of GaN to energetic ion irradiation. Based on the experimental results presented here and in ref. [7], the threshold for SHI track formation in bulk GaN was found to lie between 22.8 keV/nm and 28.3 keV/nm. After HCI irradiation, no ion tracks were observed under normal incidence even after irradiation with Xe^{40+} having a potential energy of E_{pt} = 38.5 keV and a kinetic energy of E_k = 100 keV. An analysis based on the analytical thermal spike model showed that the model parameters are in general agreement with the expected response of a semiconducting material to SHI irradiation, while the exact value of the HCI track formation threshold remains to be addressed in future experiments.

After grazing incidence SHI irradiation, ion tracks mostly in the form of chains of nanohillocks were found after 92 MeV Xe^{23+} irradiation, while only nanoholes were found after 23 MeV I^{6+}. Although here presented results indicate that SHI track formation is much easier on the surface than in the bulk, the origin of the unusual track morphology remains to be elucidated further. The appearance of nanoholes and the significant loss of nitrogen found by *in-situ* TOF-ERDA, in combination with the relatively low decomposition temperature of GaN, suggest similarities with the groove formation in SiC [54], where the predominant loss of Si is also described as a thermally driven process.

ACKNOWLEDGEMENTS

This work has been supported by the European Community as an Integrating Activity "Support of Public and Industrial Research Using Ion Beam Technology (SPIRIT)" under EC contract no. 227012. MK, MB, ZS and MJ acknowledge the Croatian Science Foundation (pr.no. 2334 and 8127) which supported this investigation. Support by the Croatian Centre of Excellence for Advanced Materials and Sensing Devices is also acknowledged.

REFERENCES

[1] Kucheyev S O, Williams J S, Pearton S J 2001 Ion implantation in GaN *Mat. Sci. Eng.* R **33** 51-107

[2] Polyakov A Y, Pearton S J, Frenzer P, Ren F, Liu L, Kim J 2013 Radiation effects in GaN materials and devices *J. Mat. Chem.* C **1** 877-887

[3] Sellin P J, Vaitkus J 2006 New materials for radiation hard semiconductor dectectors *Nucl. Instrum. Meth. Phys. Res.* A **557** 479-489

[4] Grant J, Bates R, Cunningham W, Blue A, Melone J, McEwan F, Vaitkus J, Gaubas E, O'Shea V 2007 GaN as a radiation hard particle detector *Nucl. Instrum. Meth. Phys. Res.* A **576** 60-65

[5] Kucheyev S O, Timmers H, Zou J, Williams J S, Jagadish C, Li G 2004 Lattice damage produced in GaN by swift heavy ions *J. Appl. Phys.* **95** 5360

[6] Zhang C H, Song Y, Sun Y M, Chen H, Yang Y T, Zhou L H, Jin Y F 2007 Damage accumulation in gallium nitride irradiated with various energetic heavy ions *Nucl. Instrum. Meth. Phys. Res.* B **256** 199-206

[7] Mansouri S, Marie P, Dufour C, Nouet G, Monnet I, Lebius H 2008 Swift heavy ion effects in III-V nitrides *Nucl. Instrum. Meth. Phys. Res.* B **266** 2814-2818

[8] Mansouri S, Marie P, Dufour C, Nouet G, Monnet I, Lebius H, Benamara Z 2008 Swift heavy ions effects in Gallium Nitride *Acta Electrotech.* **49** 147-150

[9] Kumar V S, Puviarasu P, Thangaraju K, Thangavel R, Baranwal V, Singh F, Mohanty T, Kanjilal D, Asokan K, Kumar J 2006 Effect of swift heavy ions of silver and oxygen on GaN *Nucl. Instrum. Meth. Phys. Res.* B **244** 145-148

[10] Kumar A, Kanjilal D, Kumar V, Singh R 2011 Defect formation in GaN epitaxial layers due to swift heavy ion irradiation *Rad. Eff. Def. Solids* **166** 739-742

[11] Wesch W, Kamarou A, Wendler E 2004 Effect of high electronic energy deposition in semiconductors *Nucl. Instrum. Meth. Phys. Res.* B **225** 111-128

[12] Itoh N, Duffy D M, Khakshouri S, Stoneham A M 2009 Making tracks: electronic excitation roles in forming swift heavy ion tracks *J. Phys.: Condens. Matter* **21** 474205

[13] Toulemonde M, Assmann W, Dufour C, Meftah A, Trautmann C 2012 Nanometric transformation of the matter by short and intense electronic excitation - Experimental data versus inelastic thermal spike model, *Nucl. Instrum. Meth. Phys. Res.* B **277** 28-39

[14] Zhang LQ, Zhang C H, Yang Y T, Han L H, Li B S, Song S J, Sun Y M, Jin Y F 2011 Potential energy threshold of surface erosion on GaN by impact of slow highly charged heavy ions *Nucl. Instrum. Meth. Phys. Res.* B **269** 396-399

[15] Akcöltekin E, Peters T, Meyer R, Duvenbeck A, Klusmann M, Monnet I, Lebius H, Schleberger M 2007 Creation of multiple nanodots by single ions, *Nature Nanotech*. **2** 290-294

[16] Akcöltekin E, Akcöltekin S, Osmani O, Duvenbeck A, Lebius H, Schleberger M 2008 Swift heavy ion irradiation of $SrTiO_3$ under grazing incidence *New J. Phys*. **10** 053007

[17] Karlušić M, Akcöltekin S, Osmani O, Monnet I, Lebius H, Jakšić M, Schleberger M 2010 Energy threshold for the creation of nanodots on $SrTiO_3$ by swift heavy ions, *New J. Phys*. **12** 043009

[18] Shrestha S K, Butcher K S A, Winterbert-Fouquet M, Timmers H 2004 Reliable ERD Analysis of group III-nitrides despite severe nitrogen depletion *Nucl. Instrum. Meth. Phys. Res.* B **219-220** 686-692

[19] Kumar V S, Kumar M S, Puviarasu P, Kumar J, Mohanty T, Kanjilal D, Asokan K, Tripathi A, Fontana M, Camarani A 2007 Investigations on the 100 MeV Au^{7+} ion irradiation of GaN *Semicond. Sci. Technol.* **22** 511

[20] Zhang L M, Zhang C H, Li C X, Song Y, Jin Y F, Wang T S 2012 Surface morphological and compositional changes of GaN films induced by swift heavy-ion irradiations *Eur. Phys. J. Appl. Phys.* **59** 30101

[21] Szenes G 2011 Thermal spike analysis of ion-induced tracks in semiconductors *Nucl. Instrum. Meth. Phys. Res.* B **269** 2075-2079

[22] Karlušić M, Jakšić M 2012 Thermal spike analysis of highly charged ion tracks *Nucl. Instrum. Meth. Phys. Res.* B **280** 103-110

[23] Aumayr F, Facsko S, El-Said A S, Trautmann C, Schleberger M 2011 Single-ion induced surface nanostructures - A comparison between slow highly-charged and swift heavy ions *J. Phys.: Condens. Matter* **23** 393001

[24] Dufour Ch., Khomenkov V, Rizza G, Toulemonde M 2012 Ion-matter interaction: the three-dimensional version of the thermal spike model. Application to nanoparticle irradiation with swift heavy ions *J. Phys. D: Appl. Phys.* **45** 065302

[25] Steinbach T, Bierschenk Th, Milz S, Ridgway M C, Wesch W 2014 Swift heavy ion irradiation of crystalline CdTe *J. Phys. D: Appl. Phys.* **47** 065301

[26] Ziegler J F, Ziegler M D, Biersack J P 2010 SRIM – The stopping and range of ions in matter *Nucl. Instrum. Methods Phys. Res.* B **268** 1818-1823

[27] Meftah A, Brisard F, Constantini J M, Dooryhee E, Hage-Ali M, Hervieu M, Stoquert J P, Studer F, Toulemonde M 1994 Track formation in SiO_2 quartz and the thermal-spike mechanism *Phys. Rev.* B **49** 12457-12463

[28] Toulemonde M, Benyagoub A, Trautmann C, Khalfaoui N, Boccanfuso M, Dufour C, Gourbilleau F, Grob J J, Stoquert J P, Constantini J M et al. 2012 Dense and nanometric electronic excitations induced by swift heavy ions in an ionic CaF_2 crystal: Evidence for two thresholds of damage creation *Phys. Rev.* B **85** 054112

[29] P. Kluth, Schnohr C S, Pakarinen O H, Djurabekova F, Sprouster D J, Giulian R, Ridgway M C, Byrne A P, Trautmann C, Cookson D J et al. 2008 Fine structure in swift heavy ion tracks in amorphous SiO_2 *Phys. Rev. Lett.* **101** 175503

[30] Toulemonde M, Webber W J, Li G, Shutthanandan V, Kluth P, Yang T, Wang Y, Zhang Y 2011 Synergy of nuclear and electronic energy losses in ion-irradiation processes: The case of vitreous silicon dioxide *Phys. Rev.* B **83** 054106

[31] Backman M, Djurabekova F, Pakarinen O H, Nordlund K, Zhang Y, Toulemonde M, Weber W J 2012 Cooperative effect of electronic and nuclear stopping on ion irradiation damage in silica *J. Phys. D: Appl. Phys.* **45** 505305

[32] Buljan M, Karlušić M, Bogdanović-Radović I, Jakšić M, Radić N, Salamon K, Bernstorff S 2012 Determination of ion track radii in amorphous matrices via formation of nano-clusters by ion-beam irradiation *Appl. Phys. Lett.* **101** 103112

[33] Bogdanović-Radović I, Buljan M, Karlušić M, Skukan N, Božičević I, Jakšić M, Radić N, Dražić G, Bernstorff S 2012 Conditions for formation of germanium quantum dots in amorphous matrices by MeV ions: Comparison with standard thermal annealing *Phys. Rev.* B **86** 165316

[34] Wesch W, Schnohr C S, Kluth P, Hussain Z S, Araujo L L, Giulian R, Sprouster D J, Byrne A P, Ridgway 2009 Structural modification of swift heavy ion irradiated amorphous Ge layers *J. Phys. D: Appl. Phys.* **42** 115402

[35] Schattat B, Bolse W, Klaumünzer S, Zizak I, Scholz R 2005 Cylindrical nanopores in NiO induced by swift heavy ions *Appl. Phys. Lett.* **87** 173110

[36] Popok V N, Jensen J, Vučković S, Mackova A, Trautmann C 2009 Formation of surface nanostructures on rutile (TiO_2): comparative study of low-energy cluster ion and high-energy monoatomic ion impact *J. Phys. D: Appl. Phys.* **42** 205303

[37] Pisarev V V, Starikov S V 2014 Atomistic simulation of ion track formation in UO_2 *J. Phys.: Condens. Matter* **26** 475401

[38] Akcöltekin S, Akcöltekin E, Roll T, Lebius H, Schleberger M 2009 Patterning of insulating surfaces by electronic excitation *Nucl. Instrum. Meth. Phys. Res.* B **267** 1386-1389

[39] El-Said A S, Heller R, Meissl W, Ritter R, Facsko S, Lemell C, Solleder B, Gebeshuber I C, Betz G, Toulemonde M et al. 2008 Creation of nanohillocks on CaF_2 surfaces by single slow highly charged ions *Phys. Rev. Lett.* **100** 237601

[40] El-Said A S, Wilhelm R A, Heller R, Facsko S, Lemell C, Wachter G, Burgdörfer J, Ritter R, Aumayr F 2012 Phase Diagram for Nanostructuring CaF_2 Surfaces by Slow Highly Charged Ions *Phys. Rev. Lett.* **109** 117602

[41] Hertkorn J, Lipski F, Brückner P, Wunderer T, Thapa S B, Scholz F, Chuvilin A, Kaiser U, Beer M, Zweck J 2008 Process optimization for the effective reduction of threading dislocations in MOVPE grown GaN using in situ deposited SiNx masks *J. Cryst. Growth* **310** 4867-4870

[42] Peters T, Haake C, Hopster J, Sokolovsky V, Wucher A, Schleberger M 2009 HICS: Highly charged ion collisions with surfaces *Nucl. Instrum. Methods Phys. Res.* B **267** 687-690

[43] Wilhelm R A, Gruber E, Ritter R, Heller R, Facsko S, Aumayr F 2014 Charge Exchange and Energy Loss of Slow Highly Charged Ions in 1 nm Thick Carbon Nanomembranes *Phys. Rev. Lett.* **112** 153201

[44] Horcas I, Fernandez R, Gomez-Rodriguez J M, Colchero J, Gomez-Herrero J, Baro A M 2007 WSXM: A software for scanning probe microscopy and a tool for nanotechnology, *Rev. Sci. Instr.* **78** 013705

[45] Amenitsch H, Bernstorff S, Laggner P 1995 High-flux beamline for small-angle x-ray scattering at ELETTRA *Rev. Sci. Instrum.* **66** 1624-1626

[46] Siketić Z, Bogdanović-Radović I, Jakšić M 2008 Development of a time-of-flight spectrometer at the Ruđer Bošković Institute in Zagreb *Nucl. Instrum. Meth. Phys. Res.* B **266** 1328-1332

[47] Siketić Z, Bogdanović-Radović I, Jakšić 2010 Quantitative analysis of hydrogen in thin films using TOF ERDA spectroscopy *Thin Solid Films* **518** 2617-2622

[48] Siketić Z, Bogdanović-Radović I, Jakšić M, Skukan N 2010 Time of flight elastic recoil detection analysis with a position sensitive detector *Rev. Sci. Instr.* **81** 033305

[49] Arstila K, Julin J, Laitinen M I, Aalto J, Konu T, Kärkkäinen S, Rahkonen S, Raunio M, Itkonen J, Santanen J-P et al. 2014 Potku – New Analysis Software for Heavy Ion Elastic Recoil Detection Analysis *Nucl. Instr. Meth. Phys. Res.* B **331** 34-41

[50] Mayer M 1997 SIMNRA User's Guide, Report IPP 9/113, Max-Planck-Institut für Plasmaphysik, Garching, Germany

[51] Buljan M et al., GISAXS characterization of ion-beam induced tracks on thin film surfaces: models and applications (in preparation)

[52] Gibbons J F 1972 Ion implantation in semiconductors – Part II: Damage production and annealing *Proc. IEEE* **60** 1062-1096

[53] Osmani O, Duvenbeck A, Akcöltekin E, Meyer R, Lebius H, Schleberger M 2008 Calculation of electronic stopping power along glancing swift heavy ion tracks in perovskites using ab initio electron density data *J. Phys.: Condens. Matter* **20** 315001

[54] Ochedowski, Osmani O, Schade M, Bussmann B K, Ban d'Etat B, Lebius H, Schleberger M 2014 Graphitic nanostripes in silicon carbide surfaces created by swift heavy ion irradiation *Nature Comm.* **5** 3913

[55] Toulemonde M, Assmann W, Trautmann C, Grüner F 2002 Jetlike component in sputtering of LiF induced by swift heavy ions *Phys. Rev. Lett.* **88** 057602

[56] Rana M A, Osipowicz T, Choi H W, Breese M B H, Watt F, Chua S J 2003 Stoichiometric and structural alterations in GaN thin films during annealling *Appl. Phys.* A **77** 103-108

[57] Stonert A, Pągowska K, Ratajczak R, Caban P, Strupinski W, Turos A 2008 Channeling study of thermal decomposition of III-N compound semiconductors *Nucl. Instrum. Meth. Phys. Res.* B **266** 1224-1228

[58] Zinkle S J, Skuratov V A, Hoelzer D T 2002 On the conflicting roles of ionizing radiation in ceramics *Nucl. Instrum. Meth. Phys. Res.* B 191 758-766

[59] Benyagoub A, Audren A 2009 Study of the damage produced in silicon carbide by high energy heavy ions *Nucl. Instrum. Meth. Phys. Res.* B **267** 1255-1258

[60] Ronchi C 1973 The nature of surface fission tracks in UO_2 *J. Appl. Phys.* **44** 3575-3585

[61] Buljan M, Grenzer J, Keller A, Radić N, Valeš V, Bernstorff S, Cornelius T, Metzger H T, Holý V 2010 Growth of spatially ordered Ge nanoclusters in an amorphous matrix on rippled substrates, *Phys. Rev*. B **82** 125316

[62] Szenes G 1995 General features of latent tracks in magnetic insulators irradiated by swift heavy ions *Phys. Rev.* B **51** 8026-8029

[63] Hopster J, Kozubek R, Krämer J, Sokolovsky V, Schleberger M 2013 Ultra-thin MoS_2 irradiated with highly charged ions *Nucl. Instrum. Meth. Phys. Res.* B **317** 165-169

[64] Szenes G 2006 Amorphous tracks induced by energetic ions in strongly anisotropic solids with layered structures *Rad. Eff. Def. Solids* **161** 401-410

[65] El-Said A S, Wilhelm R A, Facsko S, Trautmann C 2013 Surface nanostructuring of $LiNbO_3$ by high-density electronic excitations *Nucl. Instrum. Meth. Phys. Res.* B **315** 265-268

[66] El-Said A S, Heller R, Wilhelm R A, Facsko S, Aumayr F 2014 Surface modifications of BaF_2 and CaF_2 single crystals by slow highly charged ions *Appl. Surf. Sci.* **310** 169-173

[67] El-Said A S, Wilhelm R A, Heller R, Akhmadaliev Sh, Facsko S 2013 Creation of surface nanostructures in Al_2O_3 by slow highly charged ions *Nucl. Instrum. Meth. Phys. Res.* B **317** 170-173

[68] Wang YY, Grygiel C, Dufour C, Sun J R, Wang Z G, Zhao Y T, Xiao G Q, Cheng R, Zhou X M, Ren J R 2014 Energy deposition by heavy ions: Additivity of kinetic and potential energy contributions in hillock formation on CaF_2 *Sci. Rep.* **4** 5742

[69] Hopster J, Kozubek R, Ban-d'Etat R, Guillous S, Lebius H, Schleberger M 2014 Damage in graphene due to electronic excitation induced by highly charged ions *2D Mater.* **1** 011011

[70] Heller R, Facsko S, Wilhelm R A, Möller W 2008 Defect Mediated Desorption of the KBr(001) Surface Induced by Single Highly Charged Ion Impact *Phys. Rev. Lett.* **101** 096102

[71] Szenes G 2007 Temperature distribution in a swift ion-induced spike *Rad. Eff. Def. Solids* **162** 557-565

[72] Szenes G 2012 About the temperature distribution in track forming insulators after the impact of swift heavy ions *Nucl. Instrum. Meth. Phys. Res.* B **280** 88-92

[73] Szenes G 2015 Uniform behaviour of insulators irradiated by swift heavy ions *Nucl. Instrum. Meth. Phys. Res.* B, in press, http://dx.doi.org/10.1016/j.nimb.2015.01.046

[74] Szenes G 2015 Ion-induced temperature rise in various types of insulators *Rad. Eff. Def. Solids*, in press, http://dx.doi.org/10.1080/10420150.2014.996880